On the Collapse of Locally Isostatic Networks

By Vitaliy Kapko[1], M.M.J. Treacy[1], M.F. Thorpe[1], S.D. Guest[2]

[1] *Arizona State University, Department of Physics and Astronomy, P.O. Box 871504, Tempe, AZ, 85287-1504, USA*

[2] *Department of Engineering, University of Cambridge, Trumpington Street, Cambridge, CB2 1PZ, UK*

We examine the flexibility of periodic planar networks built from rigid corner-connected equilateral triangles. Such systems are locally isostatic, since for each triangle the total number of degrees of freedom equals the total number of constraints. These nets are 2D analogues of zeolite frameworks, which are periodic assemblies of corner-sharing tetrahedra. If the corner connections are permitted to rotate, as if pin-jointed, there is always at least one collapse mechanism in two dimensions (and at least three mechanisms in three dimensions). We present a number of examples of such collapse modes for different topologies of triangular net. We show that the number of collapse mechanisms grows with the size of unit cell. The collapsible mechanisms that preserve higher symmetry of the network tend to exhibit the widest range of densities without sterical overlap.

Keywords: Flexibility, Locally Isostatic Networks

1. Introduction

In this paper we examine locally isostatic periodic planar networks of corner-sharing equilateral triangles. In these networks, each triangle is connected at the corners to three neighbours, and each corner is shared between two triangles. The triangles are rigid but can freely rotate in the plane, as if pin-jointed at their corners. The networks, being periodic, are infinite in extent, but can be decomposed into finite repeated units, analogous to unit cells in crystals. By locally isostatic, we mean that for each rigid unit the number of degrees of freedom equals the number of constraints. For our plane nets, each equilateral triangle has three degrees of freedom (two translations and one rotation) and six constraints (x and y coordinates for each corner). But each corner is shared between two triangles, so the number of constraints per triangle is also three, rendering these nets locally isostatic.

The 3D analogue of these systems, networks of corner-sharing SiO_4 tetrahedra, provide a model of zeolites. These systems are also locally isostatic with six degrees of freedom per tetrahedron and twelve shared constraints. This 'rigid unit mode' model has been intensively studied by M. Dove and co-workers (Hammonds *et al.* 1997, 1998) who applied it to diffusion and adsorption in zeolites facilitated by flexibility. More recently, Sartbaeva *et al.* (2006) using geometric simulations have shown that frameworks of real zeolites can be realized at some range of densities called the 'flexibility window'. They argue that the presence of the flexibility window can be used as a criterion for the selection of potential synthetic targets among the

millions of hypothetical zeolite frameworks (Treacy *et al*, 1997, 2004; Earl and Deem, 2006).

Networks of corner-sharing triangles or tetrahedra have the same flexibility properties as pin-jointed frames made of rigid bars placed at triangle edges and connected by frictionless joints. These finite pin-jointed structures have been extensively studied. Maxwell(1864), introduced a simple rule: a system having j joints and no kinematic constraints requires at least $3j-6$ (in 3D) or $2j-3$ (in 2D) bars to be rigid. The Maxwell rule was generalized by Laman's theorem (Laman 1970), which solves the problem of generic rigidity in 2D (rigidity that depends only on the topology of the system but does not depends on the specific edge lengths nor joint coordinates). The Laman count has been implemented in the 'pebble game' by Jacobs & Thorpe (1995, 1996). This numerical algorithm can determine the rigidity of an arbitrary generic pin-jointed structure and enumerate its rigid and underconstrained regions. Unfortunately, the pebble game cannot be applied to zeolite frameworks nor to the 2D networks considered here. These systems are nongeneric and exist in symmetrical realizations that can make some constraints redundant and hence the system is not amenable to simple constraint counting.

To overcome these difficulties, one can use the linear algebra method described by Pellegrino & Calladine (1986). This method calculates the rank of the 'equilibrium' or 'rigidity' matrix and identifies infinitesimal motions in the system. These motions can be either finite (where the system can be continuously deformed without deformations of its rigid units) or infinitesimal (where there is deformation of second or higher order).

The flexibility of infinite repetitive structures is much less known. Guest & Hutchinson (2003) generalized the Pellegrino and Calladine matrix method for infinite repetitive structure. They also proved, based on a linear algebra argument, that locally isostatic infinite repetitive structures always have at least one (in 2D) or three (in 3D) internal mechanisms. More recently, Hutchinson & Fleck (2006) have classified periodic mechanisms and states of self-stress for the kagome lattice.

In this paper we extend these studies to a larger number of locally isostatic networks. We show that all the networks studied have finite mechanisms that change the volume of the unit cell.

2. Theoretical background

(*a*) *Matrix analysis and kinetic determinacy of repetitive structures*

Pellegrino & Calladine (1986) used linear algebra methods to analyze the flexibility of pin-jointed structures. They described the equilibrium matrix, $\mathbf{A}$, which relates bar tensions, $\mathbf{t}$, with external forces, $\mathbf{f}$, acting on the joints

$$\mathbf{A}\cdot\mathbf{t}=\mathbf{f}. \tag{2.1}$$

The transpose of the equilibrium matrix, the compatibility matrix, $\mathbf{C}$ connects the joint displacements, $\mathbf{d}$, with bar elongations, $\mathbf{e}$:

$$\mathbf{C}\cdot\mathbf{d}=\mathbf{e}. \tag{2.2}$$

The compatibility matrix is an n by $2j$ matrix, where n is the number of bars and j is the number of joints. The number of mechanisms, or floppy modes, f, is related

to the rank of the compatibility/equilibrium matrix r by

$$f = 2j - r. \tag{2.3}$$

For the structures that we are considering there are, on average, just the right number of constraints so that $n = 2j$, so that for local isostatic networks of the kind we talk about in this paper, the equilibrium matrix $\mathbf{A}$ in (2.1) is square and n by n. This implies that, if we consider a fixed unit cell, and write down a compatibility matrix, the matrix will also be square and n by n. The unit cell is the basic repetitive unit which contains a fixed number of nodes, edges etc and which do not change during a deformation. Thus although the area of the cell does changes, the contents do not. This repetitive unit may be just the original cell that defines the undeformed lattice itself, or an integer number of such cells in each of the two directions in the plane. However, if we now also allow the unit cell to deform, in 2D we get another 3 deformation parameters (for instance two orthogonal stretches and a shear), and the 'augmented' compatibility matrix will be n by $n+3$ (Guest & Hutchinson 2003). This matrix is guaranteed to have at least a three-dimensional nullspace (joint movements/changes in shape of the unit cell that, to first order, don't cause extension of bars/deformation of triangles). This nullspace must contain two rigid-body displacements; but this still leaves an orthogonal one-dimensional space. This space *cannot* be a rigid-body rotation, as such a motion is not allowed by the repetitive displacements demanded by the lattice; thus it must be an 'internal' mechanism. This is a subtle argument that results in at least one internal deformation for each repetitive cell. These are infinitesimal deformations, but the argument can be repeated, as the structure is still repetitive after the deformation is made, and hence leads to finite deformation(s) and pathways that are discussed in section 3 (f). Because the network is repetitive, it is infinite in extent and therefore no rotational motion is possible. This is because any such rotation would not be consistent with the repetitive nature of the structure. There are of course still the two macroscopic translational modes of deformation that can be achieved at no cost in energy and so are zero frequency or floppy modes, albeit of a trivial kind. Although the absence of rotations might seem trivial, it in fact leads indirectly to observable consequences. What would have been a rotation mode has been converted into an internal deformation, by the imposition of a repetitive structure, and indeed this in some sense the case, but it is a mathematically rigorous result, illustrated by the many examples in this paper.

There seems at first sight a contradiction here. On the one hand we are saying that we have locally isostatic networks, which are therefore rigid, while on the other hand, we are saying there is at least one internal deformation mode. The difference is that having a repetitive structure makes the network atypical, thus introducing additional floppy mode(s) or internal deformation(s). If the network was truly generic, then it would have no repetitive unit from a geometrical standpoint, and hence would indeed be rigid.

A similar argument applies in 3D, where allowing the unit cell to deform gives six deformation parameters, the augmented compatibility matrix is n by $n+6$, the nullspace must be at least 6-dimensional, three of which are simple translational degrees of freedom, which leaves at least three 'internal' mechanisms or floppy modes. Thus locally isostatic networks, like zeolites, that are made up of corner-sharing tetrahedra, have at least 3 internal deformation modes if they are repetitive,

because such networks are atypical. This leads to a rich behavior in a wide variety of silica networks (Hammonds *et al.* 1997, 1998) and in zeolites (Sartbaeva *et al.* 2006). Pathways in these networks are also finite, as infinitesimal deformations can be strung together (as in 2D), but have much more complexity, which is one motivation for this paper. Studying pathways in 2D is so much more tractable, as well as easy to visualize, as compared to 3D.

(*b*) *Ring count*

Next we rederive the simple relation between fractions of rings of different sizes. If we replace each triangle with a vertex, and consider each link between triangles as an edge, any network of corner-sharing triangles can be turned into a 3-connected net. In this paper we use the terms net and network interchangeably to describe an infinite set of vertices connected by edges. Thus 3-connected nets (or networks) are when every vertex is joined to exactly 3 other vertices by edges. For any infinite 2D-net, according to the Euler equation (Coxeter 1961), the sum of the number of vertices V and polygons (rings) P per unit cell is equal to the number of edges, $V + P = E$. If we define there to be N_n polygons with n vertices in each unit cell, then $P = \sum_n N_n$. Further, counting the vertices for every polygon, $\sum_n nN_n$, will count each vertex three times; similarly, counting the vertices for every edge, $2E$, will count each vertex three times, so that

$$3V = 2E = \sum_n nN_n. \tag{2.4}$$

Thus, substituting into the Euler equation,

$$6P = 6E - 6V \tag{2.5}$$

$$6\sum_n N_n = \sum_n nN_n \tag{2.6}$$

which means that the average ring size is six for any plane net. Thus, it is impossible to build a network that comprises only small rings (smaller than six) or only large rings. The presence of large rings in network has to be compensated by small rings.

3. Examples

(*a*) *Kagome lattice*

The simplest network of triangles, the kagome lattice (fig. 1) comprises only one type of ring, which according to (2.6) must be hexagonal (the corresponding 3-connected net is known as the 'honeycomb' net). The infinitesimal collapse mechanisms of the kagome lattice have been studied in detail by Hutchinson & Fleck (2006). With the smallest unit cell, which has the form of a rhombus with angle $\pi/3$, and consists of only two triangles, the network has only one collapse mechanism, as shown in fig. 1b. This mechanism reduces the $p6mm$ plane symmetry to $p31m$. For definitions of plane symmetry groups see (Hahn 1995). The area of the unit cell is

$$S = a^2 \sin \pi/3 = \sqrt{3}\, l^2(1 - \cos\theta), \tag{3.1}$$

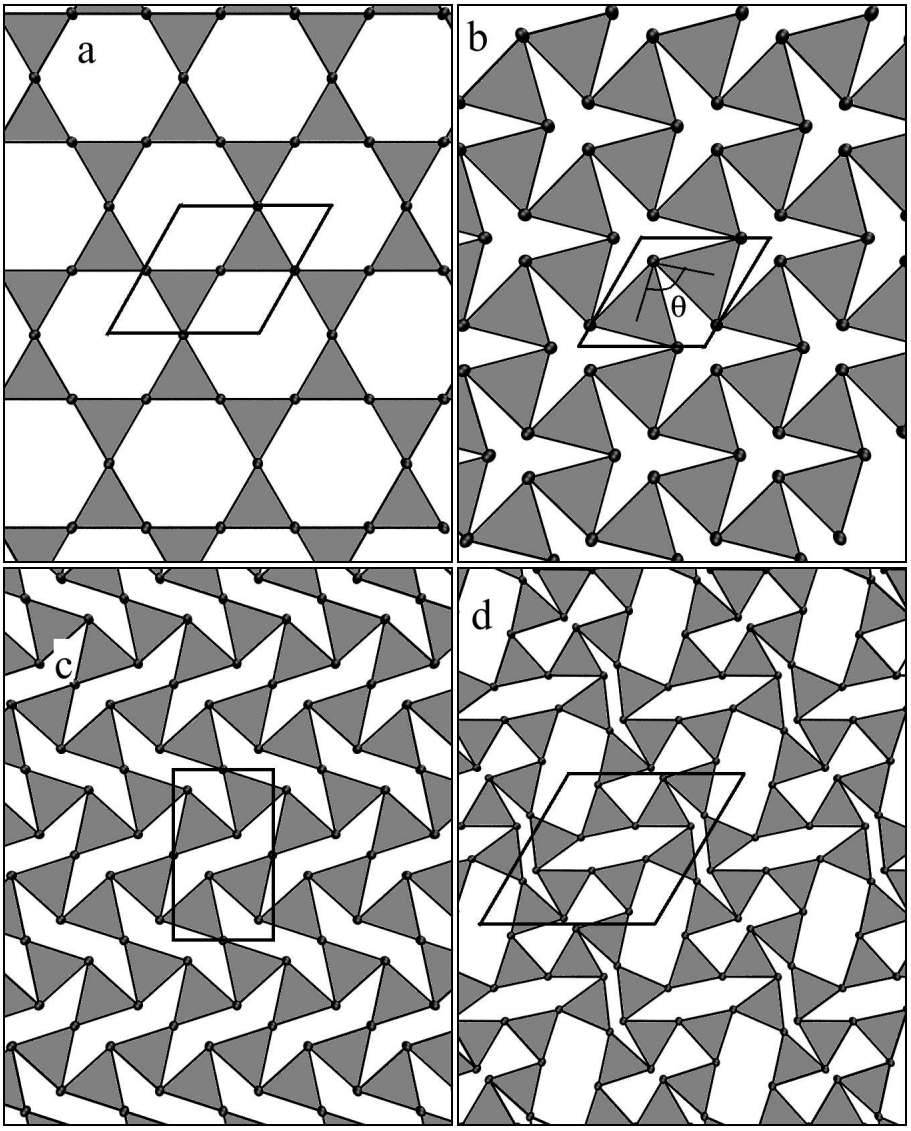

Figure 1. Four different configurations of the kagome topology. a) Minimum density state, with $p6mm$ plane group symmetry. b) Snapshot of the collapse mode available when there is one hexagon per hexagonal unit cell ($p31m$ plane group symmetry). c) Snapshot of an alternative collapse mode when there are two hexagons per rectangular unit cell ($p2gg$ plane group symmetry). d) Snapshot of an additional collapse mode when there are four topologically distinct hexagons per oblique unit cell ($p2$ plane group symmetry).

where a and l are, respectively, the length of the unit cell and the side of triangle, and θ is an angle between two lines connecting two centers of adjacent triangles. The maximal area, $S_{\max}$, occurs at $\theta = \pi$, and the value of the minimal area, $S_{\min}$, depends on whether triangles are allowed to overlap. If triangles are allowed to overlap ($\theta < \pi/3$), then the unit area vanishes at $\theta = 0$, which means that any

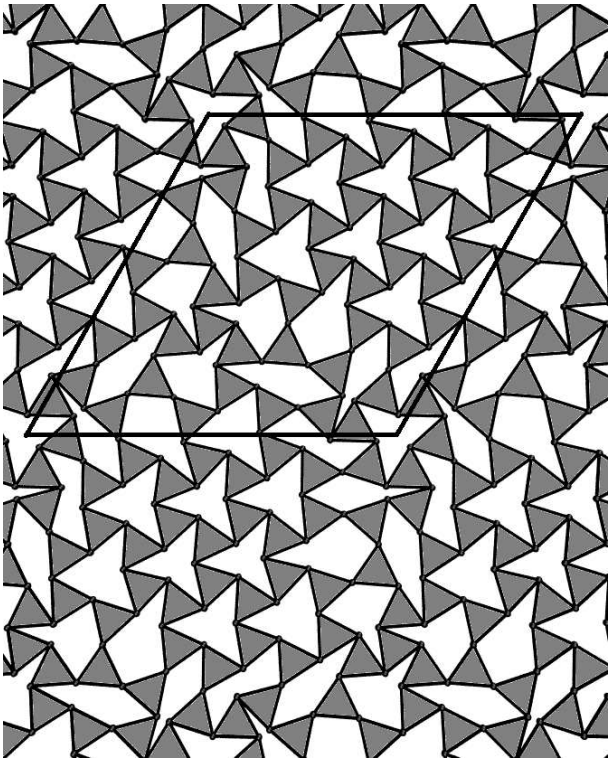

Figure 2. One collapse mechanism of the kagome net with a 5×5 unit cell ($p3$ plane group symmetry).

finite piece of a kagome lattice collapses into a single triangle, but with a unit cell of zero edge length.

The number of internal mechanisms grows as the relative size of the unit cell increases. Thus, fig. 1c shows a new mechanism (in addition to the mechanism shown in fig. 1b) that appears when the unit cell contains two rings. This mechanism adopts plane group symmetry $p2gg$, and can be transformed into the higher symmetry, and vice versa, through the configuration of maximal area (fig. 1a). The two rings are related by a glide symmetry operation and therefore have equal area, and the new mechanism does not affect the density calculation for the kagome lattice.

A further collapse mode that appears for the 2×2 unit cell is shown in fig 1d. Its unit cell has plane group symmetry $p2$, and contains four distinct hexagon configurations. The network maintains a 2-fold symmetry axis at the middle of each ring. Finally, fig. 2 shows one of the collapsing mechanisms in the kagome net with a unit cell that is a 5×5 repeat of the basic kagome cell. The plane group symmetry is $p3$, with nine topologically distinct hexagon configurations.

(*b*) *'Roman mosaic' lattice*

For the next example, we consider the net shown in fig. 3, which is made of equal numbers of rhombi and octagons (we will refer to the corresponding 3-connected

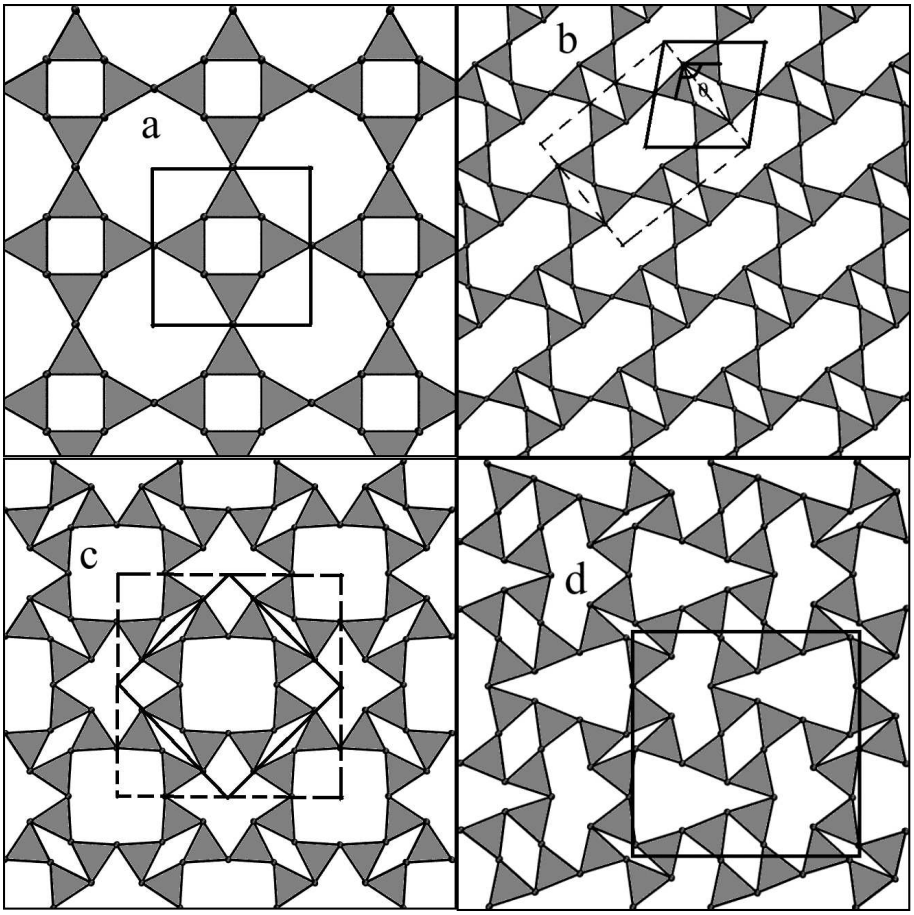

Figure 3. Roman mosaic net. a) Minimum density configuration, $p4mm$. b) Snapshot of the shear collapse mode that occurs when there is one octagon and one rhombus per primitive unit cell, $c2mm$. c) Snapshot of the high symmetry collapse mode when there are two octagons and two rhombi per square unit cell, $p4mm$. d) Snapshot of the low symmetry collapse mode when there four octagons and four rhombi per square unit cell, $p2mg$.

net as the roman mosaic lattice, as it is a tiling pattern found on Roman floors). Some of the collapse mechanisms are shown in fig. 3. Since a rhombus has only one internal degree of freedom, defined by the angle θ shown in fig. 4, we consider the 'roman mosaic' lattice as tessellations of rhombi. Within the primitive unit cell (four equilateral triangles, delineated by the solid lines) the network has only one mechanism (sheared collapse), shown in fig. 3b. There is a higher symmetry, face-centered setting $c2mm$ delineated by the dotted cell in fig. 3b. The area of the oblique primitive cell (shown by the solid lines) is equal to twice the area of the rectangle shown in fig. 4. From fig. 4, $|AB| = 2l\,\sin[\theta/2]$ and $|BC| = 2l\,\sin[\theta/2 + \pi/6]$, thus the area of unit cell, S is given by

$$S = 2|AB| \cdot |BC| = 4\,l^2\left[\sqrt{3}/2 - \cos(\theta + \pi/6)\right] \tag{3.2}$$

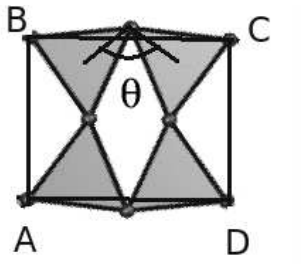

Fig

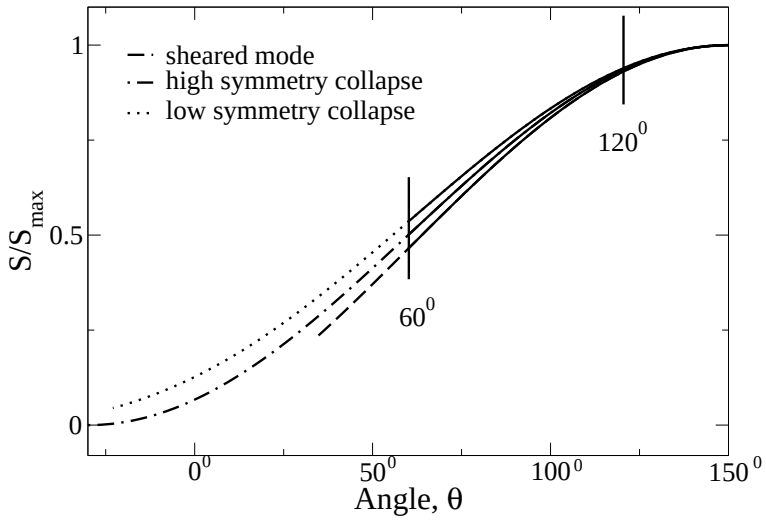

Figure 5. Normalized areas of the Roman mosaic network as a function of the inter-triangle angle in the rhombus. There is a distinct equation of state for each collapse mode. Vertical lines marked 60° and 120° indicate the angles where triangles and oxygens touch (see subsection *Flexibility index* for details).

The area has maximum at $\theta = 5\pi/6$ which equals to $S_{\max} = 2\,l^2\,(2+\sqrt{3})$ and minimum at $\theta = \pi/3$ with $S_{\min} = 2\sqrt{3}\,l^2$.

Two other collapse mechanisms can be found when the unit cell remains square, but now contains eight triangles. The mechanism shown in fig. 3c (symmetric collapse) can be presented as columns (or rows) of rhombi connected through mirror lines. The unit cell splits into two rectangles with sides equals to $|AB|$ and $|BC|$ and two squares, one with side $|AB|$ and the other with side $|BC|$. Then the unit cell area is

$$S = 2\,|AB|\cdot|BC| + |AB|^2 + |BC|^2 = 2\,l^2\,(2+\sqrt{3})\,(1-\cos[\theta+\pi/6]). \qquad (3.3)$$

The maximal area is $S_{\max} = 4\,l^2(2+\sqrt{3})$ and the minimum area is exactly half this, $S_{\min} = 2\,l^2(2+\sqrt{3})$

The last mechanism considered here (asymmetric collapse, fig. 3d) can be viewed

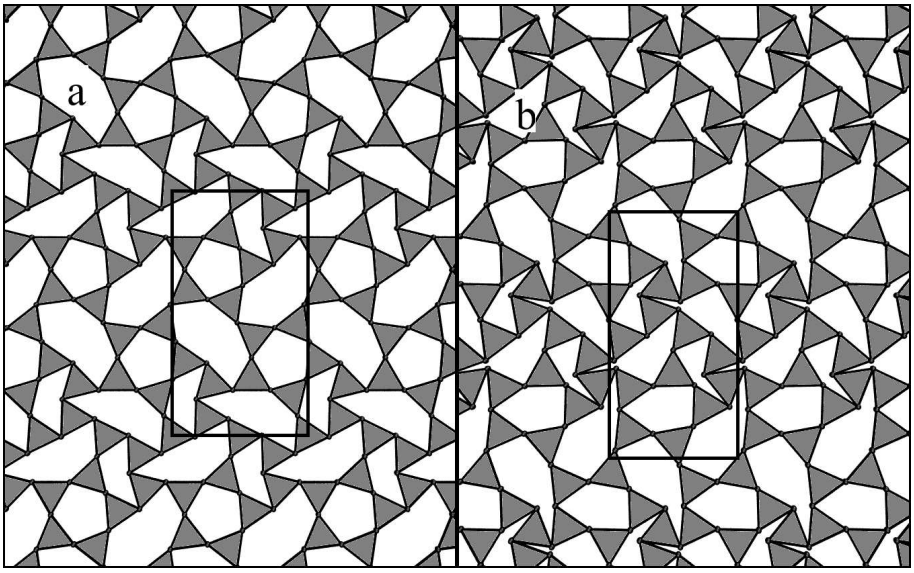

Figure 6. A network with only odd rings, 5-rings and 7-rings in equal numbers. a) Minimum density state (maximum area), and b) an intermediate density state. This net maintains *pg* plane group symmetry during deformation.

as rows of rhombi with two different, alternating, sizes. The unit cell area for this case has been solved numerically.

Figure 5 shows the dependency of the area of one unit cell of the Roman mosaic on the angle θ for different collapsing mechanisms. The solid lines correspond to the region where triangles do not overlap ($\theta > \pi/3$). The shear mechanism shows larger changes in unit cell area than the others. Once overlap between triangles is allowed the structures continue to shrink until the entire infinite net collapses at $\theta = 0$ into a finite structure of a few triangles (similar to the collapse of the kagome lattice). The angle θ is zero when adjoining equilateral triangles lie exactly on top of each other. The dashed line corresponding to the sheared mode stops at $\theta = 34°$. At this point the system flips to the other configuration as it is shown at fig. 9 and continues to collapse to zero area configuration with angle θ fixed at $\pi/3$.

(*c*) *Network with odd rings*

Both the kagome and Roman mosaic networks have even numbers of triangles in each ring, and also have high symmetry, which may increase the number of infinitesimal mechanisms (Guest, 2000) by making constraints redundant. Flexibility is not restricted to structures with even rings. The network shown in fig. 6 comprises only odd rings (sizes 5 and 7), with a rectangular unit cell of plane group symmetry *pg*, and containing 16 equilateral triangles. Figure 6a presents the maximal area configuration, and fig. 6b demonstrates a collapse mechanism that retains the rectangular symmetry of the unit cell, but alters its aspect ratio.

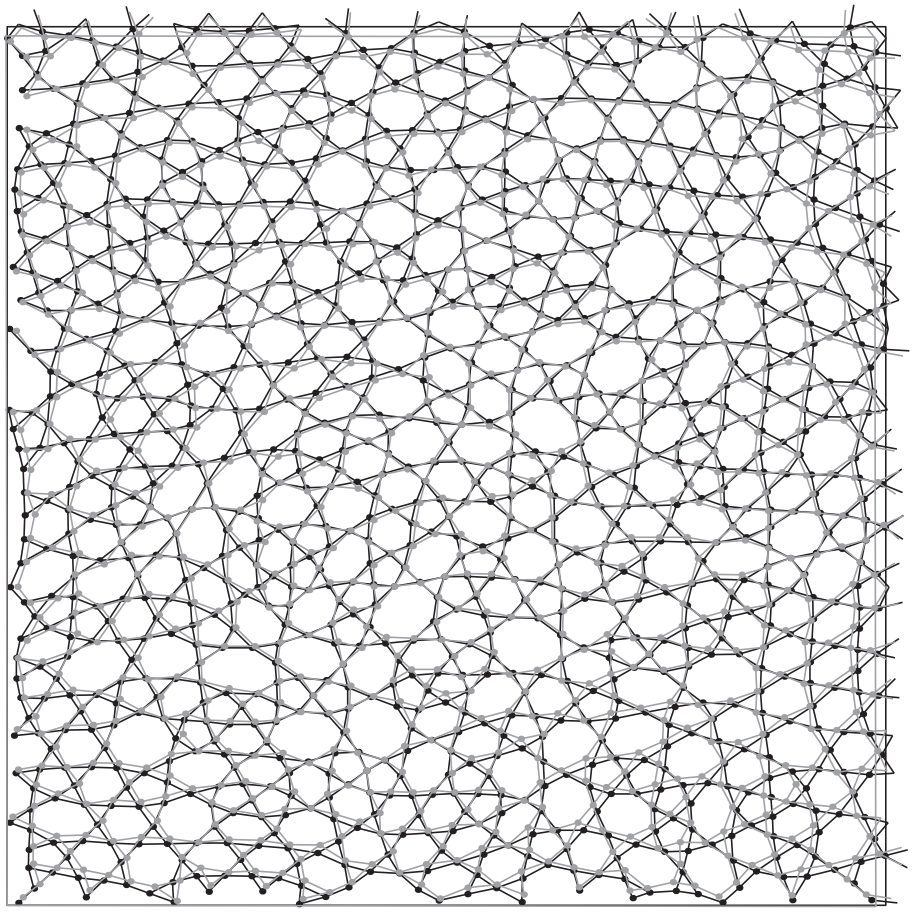

Figure 7. A large random network. Two states are superimposed; the unit cell of the state shown in grey has an area just over 2% smaller than the state shown in black.

(*d*) *Large random network*

Our last example, a large random network shown in fig. 7, is taken from computer modeling of vitreous silica (He, 1985). This periodic structure was generated by successively introducing 250 defects into an 800-site honeycomb lattice, while maintaining full corner connectivity. The network contains 33.5% pentagons, 24% heptagons and 4.5% octagons and appears disordered. A first order calculation shows that this network has one infinitesimal collapse mode, and following this path gives an alternative finitely deformed configuration, which is also shown superimposed in the figure.

(*e*) *Flexibility index*

As a way to measure network flexibility we introduce a flexibility index

$$F = S_{\max}/S_{\min}. \tag{3.4}$$

Lattice	Mechanism	F_Δ	F_O
kagome	1×1 (fig. 1b)	4	1.333
	2×1 (fig. 1c)	4	1.333
	2×2 (fig. 1d)	2	1.180
	5×5 (fig. 2)	2.187	1.135
Roman mosaic	sheared (fig. 3b)	2.155	1.077
	symmetric collapse (fig. 3c)	2	1.072
	asymmetric collapse (fig. 3d)	1.862	1.066
5×7 net	fig. 6b	1.553	1.090

Table 1. Flexibility indices for different collapse mechanisms of various lattices.

The maximum area, S_max, is defined as the area where triangles are under tension and would start stretching if the area were increased further. We use two different definitions for the the minimum area, S_min. In one definition the minimum area occurs when triangles first touch, which corresponds to the density where the smallest angle θ_min equals $\pi/3$. The other option for the minimum area is related to the definition of the flexibility window in 3D zeolite frameworks (Sartbaeva *et al.* 2006). According to this, each vertex is occupied by an oxygen atom with radius equal to half of the triangle side. Then the minimum area, defined by the touching of oxygen atoms, occurs when the smallest angle equals $\theta_\mathrm{min} = 2\pi/3$. Both definitions give rise to flexibility indexes, the former F_Δ and the latter F_O, and these are presented in table 1 for different frameworks and their collapse mechanisms. From the definition of the flexibility indices, it is clear that the larger they are, the more flexible is the framework. For rigid structures the flexibility indices equal unity.

(*f*) *Collapse of networks without repulsion*

In this section we take one further step in our modeling these 2D isostatic networks and assume that there is no repulsion between triangles or between vertices. In this purely theoretical situation, compression of the network will continue until the unit cell area becomes zero. In that case all triangles are laying on the top of each other and the entire infinite network becomes a very small system of few (in some cases just one) triangle(s). In the simplest case, the basic collapse mechanism of kagome lattice shown on fig. 1 b), the network can be continuously folded from the point of maximum area (fig. 1 a) to the point of zero area by changing the angle θ from π to 0. At the $\theta = 0$ point all periodic images of vertices coincide with each other and whole system is reduced to a single triangle. However, there is a second way to collapse the system. It also starts from the maximum area configuration and proceeds by increasing θ from π to 2π. It is easy to see that the final configuration is again just a single triangle but each intermediate point is the same as in the previous pathway, but related by a symmetry operation. Since the two paths intersect with each other only at two points – maximum and zero areas – they can be combined into one continuous closed pathway, as shown in fig. 8a. The pathways shown in fig 8a use the area S as the radius in polar coordinates, and uses θ as the usual angle in polar coordinates. For the kagome lattice, the basic collapse pathway has the form of a cardioid given by (3.1).

As was mentioned before, the 1×1 kagome lattice has only one folding-unfolding

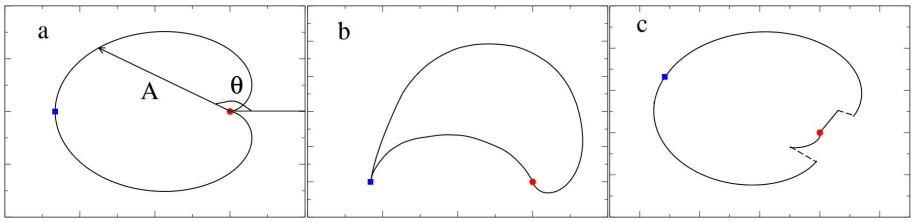

Figure 8. The 'pathway' plot of unit cell area S shown as the length of the radius vs inter-triangle angle θ in polar coordinates. a) 1×1 kagome net, b) 2×2 kagome net, c) shear collapse mode of Roman mosaic net. The solid blue rectangle and the solid red circle represent the maximum and zero areas.

path. With increasing size of the unit cell, new collapse modes appear. Fig 8b represents one of such modes in the 2×2 kagome lattice. This pathway has the shape of a highly deformed cardioid. In both cases above, the fundamental unit cells keep their shape ($a = b$, $\gamma = \pi/3$) during compression and at the zero area $a = b = 0$.

It turns out that the collapse pathways of two other systems, the 2×1 kagome (fig. 1c) and the Roman mosaic net high symmetry collapse, also have form of a cardioid. For the Roman mosaic low-symmetry collapse it is a deformed cardioid. However, this is not the case for all networks. An interesting example is the shear mode of the Roman mosaic (fig. 3b). Again, we consider the pathway of the unit cell area S as a function of an intertriangle angle θ. At the maximum area angle $\theta = 5\pi/6$. Similar to previous cases, there are two collapse paths related to decreasing or increasing of θ. At some density, both paths have a discontinuity, shown with dashed lines on fig. 8c. At that density the system cannot continue to follow the folding path without violation of geometric constraints, so instead the system flips to another configuration that has the same density. Both configurations, before and after the flip, are shown on fig 9b and 9c. After the flip the system collapses to zero area, which has a shape of two adjusted triangles (fig. 9d). During the compression $a = b$ and these go to zero as the area goes to zero. The angle γ decreases from $\pi/2$ to about $2\pi/9$ before the flip and remains fixed at $\pi/3$ after it.

We note that results in this section are often different if a different angle is chosen to display the pathway, and we have found no objective way of selecting which angle to display. The ones shown here give particularly 'simple' closed pathways as shown in the three panels of fig 8.

4. Conclusions

We have tested the argument contained in Guest & Hutchinson (2003) about collapsible mechanisms in repetitive, locally isostatic, structures. According to this argument, such structures are collapsible with, at least, one mechanism for plane nets and at least three mechanisms for 3D nets. Our examples are 2D networks of corner-sharing triangles ranging from the kagome lattice, which is the simplest network containing rings of only one size, up to the large random network with 800 triangles. We show that all these structures are flexible. The number of collapse mechanisms grows with the size of the unit cell. But this is still the subject

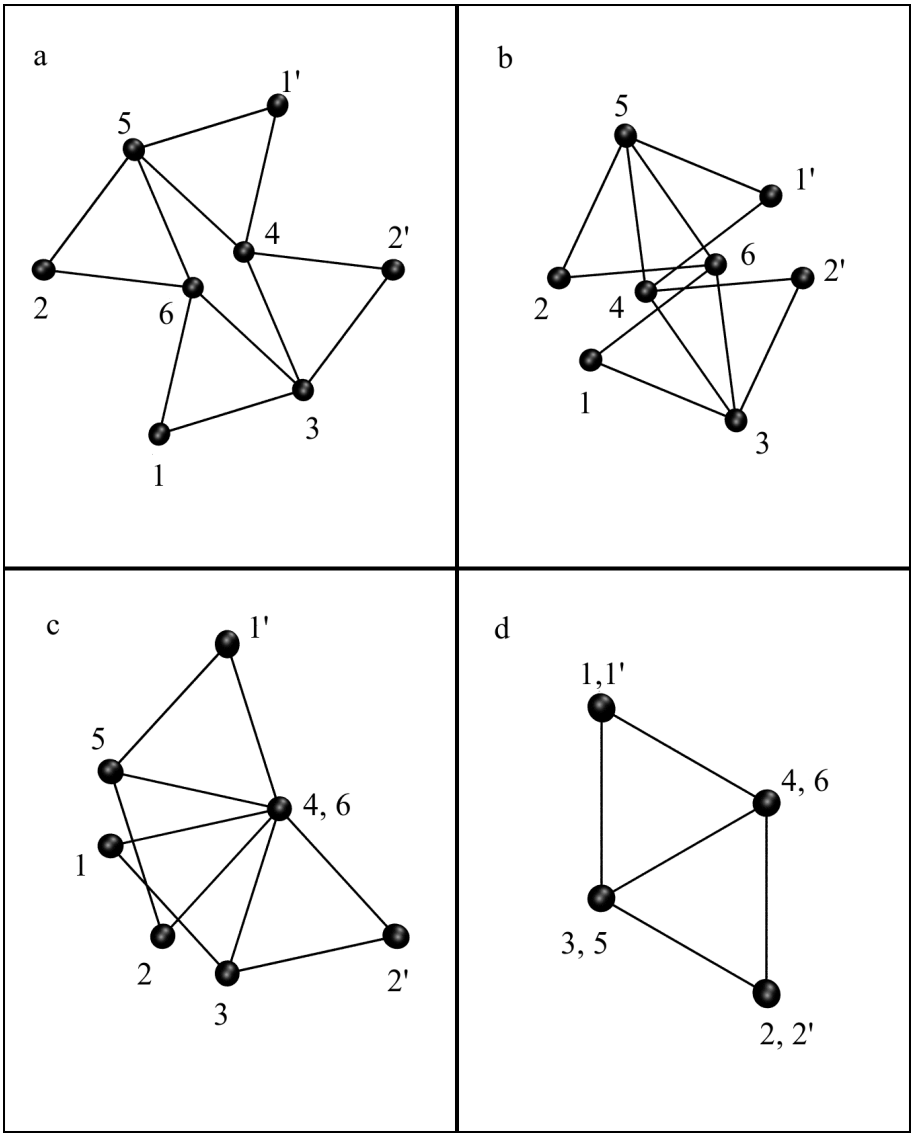

Figure 9. Illustration of the flip associated with the shear mode of Roman mosaic. a) some large area configuration, b) before flip, c) after flip, d) zero area. Each vertex is labeled with an integer number. Vertices 1' and 2' are periodic images of vertices 1 and 2.

of ongoing work. Results do appear for the number of infinitesimal modes for particular systems, in e.g. Hutchinson & Fleck (2006), and Hammonds et al. (1998), but no general rule has been found, nor is there any understanding of how these infinitesimal modes might extend to finite deformations. We have also found that the collapsible mechanisms that preserve the higher symmetry of the network tend to exhibit the widest range of densities without sterical overlap.

This paper was initially developed at the workshop 'Geometric constraints with applica-

tions in CAD and biology', organised by Ileana Streinu at Bellairs Research Institute. We acknowledge useful discussions with B. Servatius, H. Servatius and W. Whiteley. We also acknowledge the financial support of the National Science Foundation grants no. DMR-0703973 and DMS-0714953, and the Donors of the American Chemical Society Petroleum Research Fund for partial support of this research.

References

Coxeter, H. S. M. 1961 *Introduction to geometry.* New York: John Wiley.

Earl, D. J. & Deem, M. W. 2006 Toward a Database of Hypothetical Zeolite Structures. *Ind. Eng. Chem. Res.* **45**, 5449–5454.

Guest, S.D. 2000. Tensegrities and rotating rings of tetrahedra: a symmetry viewpoint of structural mechanics. *Philosophical Transactions of the Royal Society of London, Series A* **358**, 229–243.

Guest, S.D. & Hutchinson, J.W. 2003 On the determinacy of repetitive structures. *J. Mech. Phys. Solids* **51**, 383–391.

Hammonds, K. D. & Deng, H. & Heine, V. & Dove M. T. 1997 How Floppy Modes Give Rise to Adsorption Sites in Zeolites. *Phys. Rev. Lett.* **78**, 3701–3704.

Hammonds, K. D. & Heine, V. & Dove M. T. 1998 Rigid-Unit Modes and the Quantitative Determination of the Flexibility Possessed by Zeolite Frameworks. *J. Phys. Chem. B* **102**, 1759–1767.

Hahn, T. 1995 *International Tables for Crystallography. Volume A.* Dordrecht/Boston/London: Kluwer Academic Publishers.

He, H. 1985 Computer generated vitreous silica networks and elastic properties of glasses. Ph.D. thesis, Michigan State University.

Hutchinson, R. G. & Fleck, N. A. 2006 The structural performance of the periodic truss. *J. Mech. Phys. Solids* **54**, 756–782.

Jacobs, D. J. & Thorpe M. F. 1995 Generic rigidity percolation: The Pebble Game. *Phys. Rev. Lett.* **75**, 4051–4054.

Jacobs, D. J. & Thorpe M. F. 1996 Generic rigidity percolation in two dimensions. *Phys. Rev. E.* **53**, 3682–3693.

Laman, G. 1970 On graphs and rigidity of plane skeletal structures. *J. Engrg. Math.* **4**, 331–340.

Maxwell, J. C. 1864 On the calculation of the equilibrium and stiffness of frames. *Phil. Mag.* **27**, 294–299.

O'Keeffe M. & Hyde B. G. 1980 Plane Nets in Crystal Chemistry. *Phil. Trans. R. Soc. A* **295**, 553–618.

Pellegrino, S. & Calladine, C. R. 1986 Matrix analysis of statically and kinematically indeterminate frameworks. *Int. J. Solids Struct.* **22 (4)**, 409–428.

Sartbaeva, A. & Wells, S.A. & Treacy, M. M. J. & Thorpe, M. F. 2006 The flexibility window in zeolites. *Nature Mat.* **5**, 962–965.

Treacy, M. M. J. & Randall, K. H. & Rao, S. & Perry, J. A. & Chadi, D. J. 1997 Enumeration of Periodic Tetrahedral Frameworks. *Z. Krist.* **212**, 768–791.

Treacy, M. M. J. & Rivin, I. & Balkovsky, E. & Randall, K. H. & Foster, M. D. 2004 Enumeration of Periodic Tetrahedral Frameworks. II. Polynodal Graphs. *Microporous and Mesoporous Materials* **74**, 121–132.